PKM2 regulates angiogenesis by local ATP production in endothelial cells

Jesús Gómez Escudero

15 de Septiembre de 2017

Fundación Centro Nacional de Investigaciones Cardiovasculares Carlos III

Departamento de Fisiología y Farmacología-Universidad de Salamanca

Angiogenesis is the formation of new blood vessels from pre-existing ones. This process begins with the reception by the endothelial cells of a stimulus that triggers the angiogenic response (Carmeliet and Jain, 2011). For that purpose, one endothelial cell, called tip cell, is activated and begins to migrate in direction of the stimulus, with the other cells of the vessel (stalk cells) following it (Tung and Tattersall, 2012). Several cell mechanisms are implicated at this initial step, as the reorganization of endothelial junctions, the migration of the tip cell by generating cytoskeletal protrusions called filopodia, and the proliferation of the stalk cells. The impairment of these processes avoid a suitable angiogenesis process (Carmeliet et al, 1999; Vitorino et al, 2015; Serra et al, 2015).

The activation of the endothelial cells induces an increase of the metabolism that is crucial, as its inhibition blocks angiogenesis (deBock et al, 2013; Verdegem et al, 2014; Yu et al, 2017). Glycolysis is the main metabolic pathway to obtain energy by the synthesis of ATP in the endothelial cells (Polet and Feron, 2013), and has several steps that regulate the flux to allow the production of energy, and to provide the other metabolic pathways with intermediate metabolites of the glycolysis (deBerardinis et al, 2010; Eelen et al, 2015). Moreover, all the cell mechanisms that allow the growth of the new vessel (endothelial cell junction, migration and proliferation) need an

efficient support of ATP to work efficiently (Van Daele et al, 1992; Moreno et al, 2014).

Cell metabolism is not homogenous as several enzymes can be compartmentalized in order to function in a more effective way (Menard et al, 2014) since the diffusion of ATP through the cell is not fast enough to provide energy for processes that occur in specific places of the cell (Jones, 1986; Hu et al, 2016). Local ATP production can regulate endothelial cell dynamics, the establishment of new cell-contacts, the movement of vesicles through cytoskeletal structures, or the reorganization of the cytoskeleton (Zala et al, 2013; deBock et al, 2013; Moreno et al, 2014).

Pyruvate Kinase (PK) is a key regulatory enzyme that catalyzes the last step of the glycolysis. PK has three forms, L (liver), R (erythrocytes) and M (muscle). This last form is the one expressed in the majority of the organs in human, and has two isoforms M1 and M2, which differ in the regulation of their catalytic activity, as PKM1 is constitutively active and PKM2 can be regulated from a more inactive to a more active form (Yamada et al, 1990; Noguchi et al, 1986; Mazurek, 2011; Anastasiou et al, 2011).

M2 isoform has a robust implication in several pathologies as cancer or inflammation (Christofk et al, 2008; Israelsen et al 2013). For this reason it has been investigated mainly in cancer cells, but there are however scarce studies in endothelial cells or angiogenesis (Li et al, 2014; Xu et al, 2015; Boeckel et al, 2016). As regulation of metabolism is crucial for angiogenesis, we decided to investigate the role of PKM2 in this process.

PKM2 regulation of endothelial cell processes implicated in angiogenesis

We began analyzing which is the main isoform of PK expressed in endothelial cells and its role in regulating some cell processes implicated in angiogenesis. PKM2 is the predominant Pyruvate kinase isoform in human endothelial cells (HUVECs) as compared with brain and lung lysates which have predominant expression of PKM1 or PKM2 respectively (Taniguchi et al, 2015) (Fig1A).

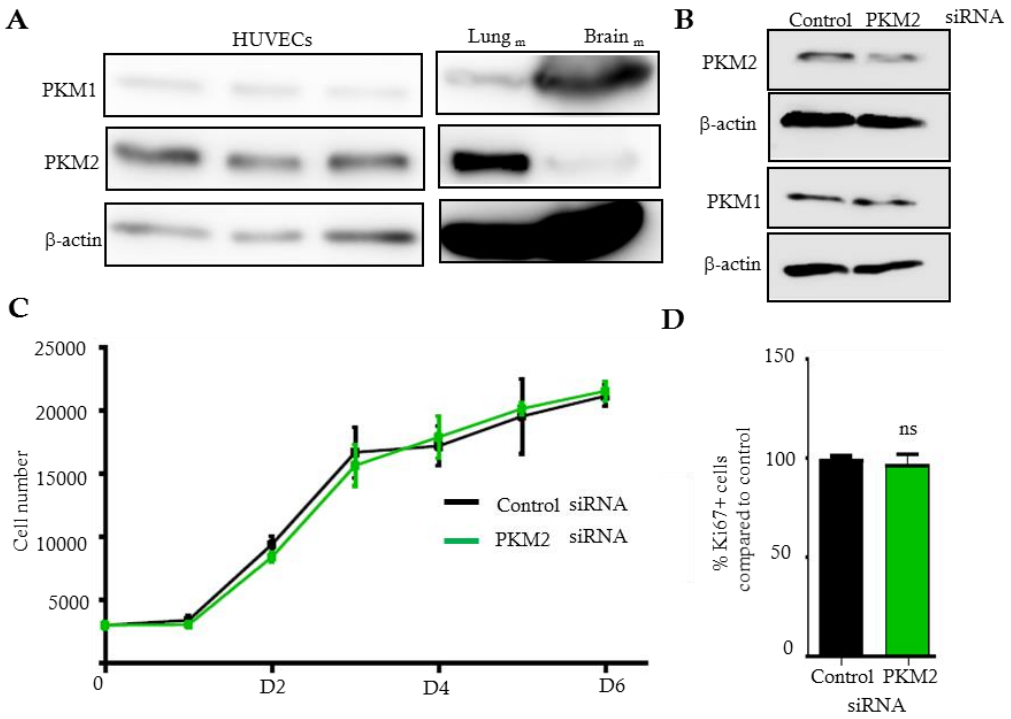

Figure1. PKM2 is the predominant PKM isoform in endothelial cells, and is dispensable for proliferation. A) Western blot analysis of HUVECs lysates. Lung and brain lysates from mouse (m) were used as positive controls of M1 and M2 isoforms. **B,** Western blot analysis of HUVECs lysates from M2 siRNA interfered cells. PKM2 and PKM1 expression was analyzed and β-actin was used as loading control. **C,** Proliferation curve of HUVECs along the time (D: day) n=4. **D,** Percentage of Ki67+ cells normalized to siRNA control HUVECs. n=3. ns= no significant.

To analyze the role of PKM2 in endothelial cell processes we interfered HUVECs with a specific M2 siRNA (Fig 1B). We found that PKM2 expression is dispensable for the proliferation of endothelial cells, as the cell number along the days and the percentage of Ki67+ cells did not change in the interfered cells (Fig 1C-D).

Next, we studied the migration capacity of HUVECs interfered for PKM2 by the scratch assay, obtaining that the interference reduced the percentage of wound closure (Fig2A-B). We demonstrated that this effect is independent from proliferation as the percentage of Ki67+ cells was the same in the assay, and as the wound closure defect was maintained in cells treated with mitomycinC, an inhibitor of cell proliferation (Fig2C-D).

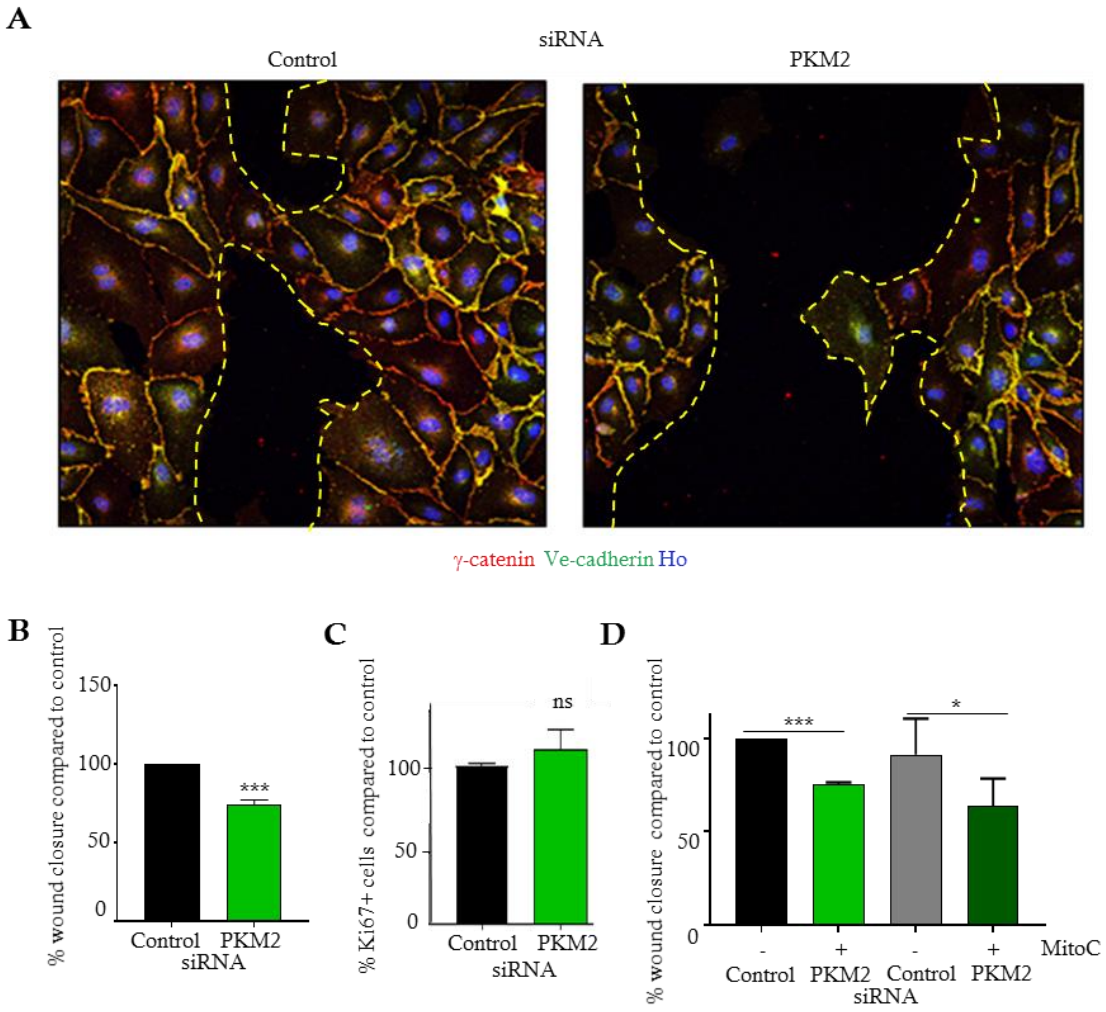

Figure 2. PKM2 affects endothelial cell migration. A, Representative maximal projections of confocal images at the final point of scratch assay. The remaining wound is delimited with a yellow line. **B**, Quantification of percentage of wound closure compared with the initial time of the assay. The result was normalized to the control siRNA cells. n=7 **C,** Quantification of percentage of Ki67+ cells at the last time point of the scratch assay. The result was normalized to the control siRNA cells. n=3. **D**, Quantification of percentage of wound closed compared with the initial time of the assay, in cells treated with 2 mg/ml of mitomycinC. The result was normalized to the non-treated control siRNA cells. n=4. ns=no significant; * p<0,05; ***p<0,001.

As the regulation of endothelial cell junction is a key point for angiogenesis and it can also be implicated in the collective migration (Hayer et al, 2016), we analyzed the role of PKM2 in this process. The interference of PKM2 impairs the intensity of Ve-cadherin, the main protein of adherens junction in HUVECs, without altering its protein expression. PKM2 silencing also changed junction morphology reflected by an increase in the proportion of discontinuous junctions, in which Ve-cadherin pattern is perpendicular to the membrane (Figure 3A-D). This phenotype also occurs in a junction-reorganization context, as is the treatment with sphingosine 1-phosphate (S1P) (Xu et al, 2007) and it is extended to other junction proteins as shown by the plakoglobin staining (Figure 3E-J). Since the impairment of endothelial cell junctions can compromise collective migration (Hayer et al, 2016), we analyzed the orientation of the cells to the wound by the polarization of the Golgi apparatus using GM130 as a marker of that organelle (Millarte and Farhan, 2012). PKM2 siRNA interfered cells increased the percentage of wrongly-oriented cells (Figure 3K-L). Since the morphology of Ve-cadherin is a parameter that can affect the endothelial barrier function, we studied the transendothelial electrical resistance (TEER) values in the interfered cells, using S1P treatment as it promotes an increase of that parameter. While the S1P-treated control cells incremented the TEER values after the stimulus, the interfered cells had a milder change leading to a worse endothelial barrier regulation (Figure 3M).

Role of PKM2 in sprouting

To analyze if the defects in EC processes caused by PKM2 interference had an implication in angiogenesis, we used first an in vitro sprouting approach, the microbead assay in fibrin gels (Nakatsu et al 2003) along six days, testing the interference at final assay day (Figure 4A-B).

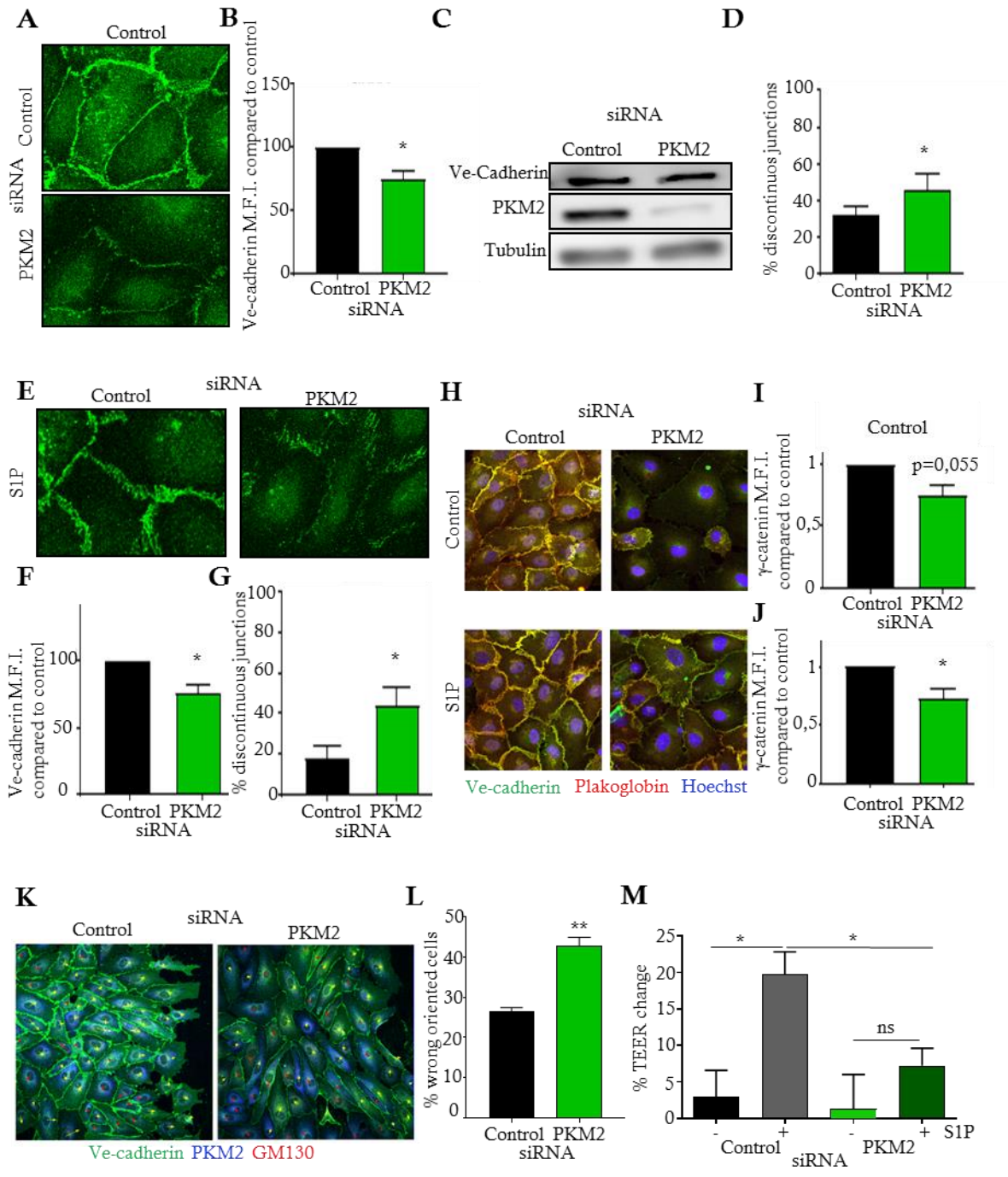

Figure 3. PKM2 regulates endothelial junction dynamics. **A**, Representative maximal projections of confocal images of confluent HUVECs interfered for PKM2 or with a control siRNA, stained for Ve-cadherin. **B**, Quantification of Ve-cadherin mean fluorescent intensity (M.F.I), normalized to control siRNA. n=5. **C**, Representative western blot of Ve-cadherin, PKM2, and β-actin from lysates of HUVECs interfered for PKM2. **D,** Quantification of percentage of discontinuous junctions in PKM2-interfered HUVECs. n=3. **E**, Representative maximal projections of confocal images of confluent HUVECs treated with sphingosine 1-phosphate (S1P) 1μM for 15 min, interfered for PKM2 or with a control siRNA, stained for Ve-cadherin. **F**, Quantification of Ve-cadherin mean fluorescent intensity (M.F.I) in HUVECs treated with S1P, normalized to control siRNA. n=4. **G**, Quantification

of percentage of discontinuous junctions in PKM2-interfered HUVECs treated with S1P. n=4. **H**, Representative maximal projections of confocal images of confluent HUVECs interfered for PKM2 or with a control siRNA, stained for Ve-cadherin (green) and Plakoglobin (red) treated or not with S1P. **I**, Quantification of Plakoglobin mean fluorescent intensity (M.F.I) in HUVECs in basal situation, normalized to control siRNA. n=3. **J**, Quantification of Plakoglobin mean fluorescent intensity (M.F.I) in HUVECs treated with S1P, normalized to control siRNA. n=3. **K**, Representative maximal projections of confocal images of HUVECs in the scratch assay interfered for PKM2 or with a control siRNA, stained for Ve-cadherin (green), PKM2 (blue) and GM130 (red). **L**, Percentage of wrongly-oriented cells from experiment in K; n=3. **M**, Quantification of percentage of transendothelial electrical resistance change after the treatment with S1P in HUVECs interfered for PKM2. ns=no significant; * p<0,05; **p<0,01

The beads covered by PKM2 siRNA HUVECshad a reduction in the number and length of sprouts, without defects in cell proliferation (Figure 4C-G). The number of filopodia, cytoskeletal structures important for sprout development (Fantin et al, 2015) was also decreased (Figure 4H-I). Finally, we classified the morphology of junctions in the sprouts using a software called "patching algorithm". This program allows you to distinguish patches of Ve-cadherin staining from more discontinuous (active) to more continuous (inactive). A correct sprouting process requires a mosaic of types of patches (Bentley et al, 2014). The sprouts from interfered endothelial cells had an accumulation of active patches that results in a significant increase in the proportion of them compared to control siRNA sprouts as shown by the active/inactive patch ratio (Figure 4J-L).

PKM2 promotes local ATP production at EC junction

Recently it has been reported the compartmentation of proteins to regulate specific processes in particularly regions of the cell (Zala et al, 2013; deBock et al, 2013; Moreno et al, 2014). For that we investigated the subcellular localization of PKM2 in endothelial cells. A pool of PKM2 localizes at endothelial cell junction, regions in which Ve-cadherin is distributed (Figure 5A). Notably we could follow PKM2 dynamics with a GFP-PKM2 construction at the junction in response to the remodeling produced by S1P (Figure 5B) and observed that PKM2 is also in the same places than the F-actin associated to endothelial junctions (Figure 5C). We checked the localization in the sprout assay, and confirmed that PKM2 is located at endothelial junction and also at the filopodia (Figure 5D-F). Finally we confirmed

the membrane localization of PKM2 by subcellular fractionation of cytosol and membrane (Figure 5G) and that it is indeed present at the plasma membrane in a subfractionation of the cell membranes by density gradient (Figure 5H).

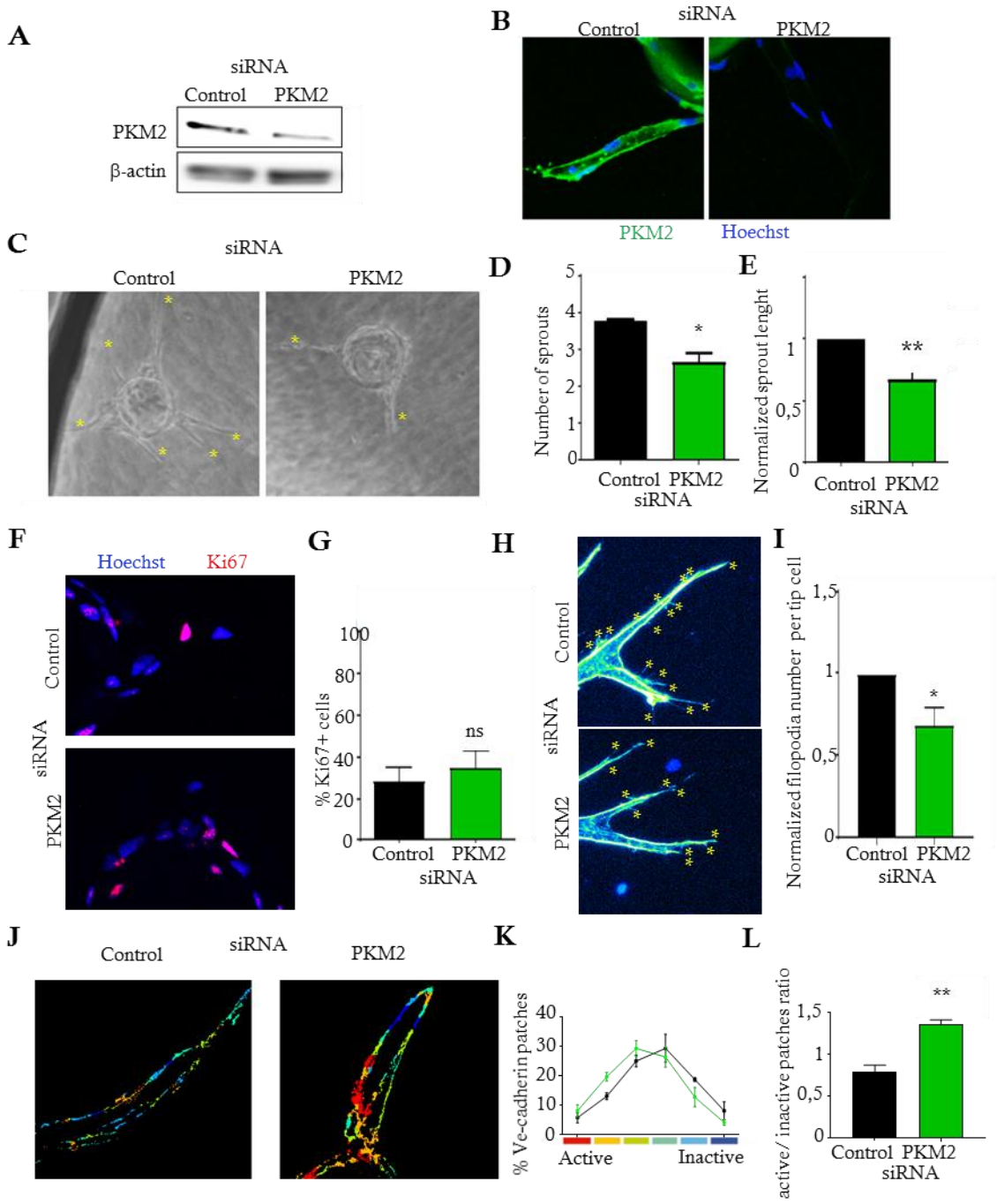

Figure 4. PKM2 regulation of endothelial cell processes in an "in vitro" angiogenesis model. **A**, Representative western blot of HUVECs interfered for PKM2 at the final day of experiment. **B**, Representative maximal projections of confocal images of sprouts of HUVECs interfered for PKM2

or with a control siRNA, stained for PKM2. **C**, Representative images of brightfield microscopy of spheroids of HUVECs interfered for PKM2. **D**, Quantification of number of sprouts in the spheroids; n=3. **E**, Quantification of sprout length normalized to control siRNA in the spheroids experiment; n=3. **F**, Representative maximal projections of confocal images of sprouts of HUVECs interfered for PKM2 or with a control siRNA, stained for Ki67. n=3. **G**, Quantification of percentage of Ki67 cells in the sprouts; n=3. **H**, Representative maximal projections of confocal images of sprouts of HUVECs interfered for PKM2 or with a control siRNA, stained for F-actin, showing filopodia with the asterisk in yellow. I, Quantification of filopodia number per tip cell normalized to control siRNA; n=5. **J**, Representative maximal projections of confocal images of sprouts of HUVECs interfered for PKM2 or with a control siRNA, stained for Ve-cadherin, showing patching algorithm reconstruction of Ve-cadherin pattern from more active (red) to more inactive (blue). **K**, Quantification of percentage of the different patches; n=3. **L**, Quantification of active/inactive patch ratio; n=3. ns=no significant; * p<0,05; **p<0,01

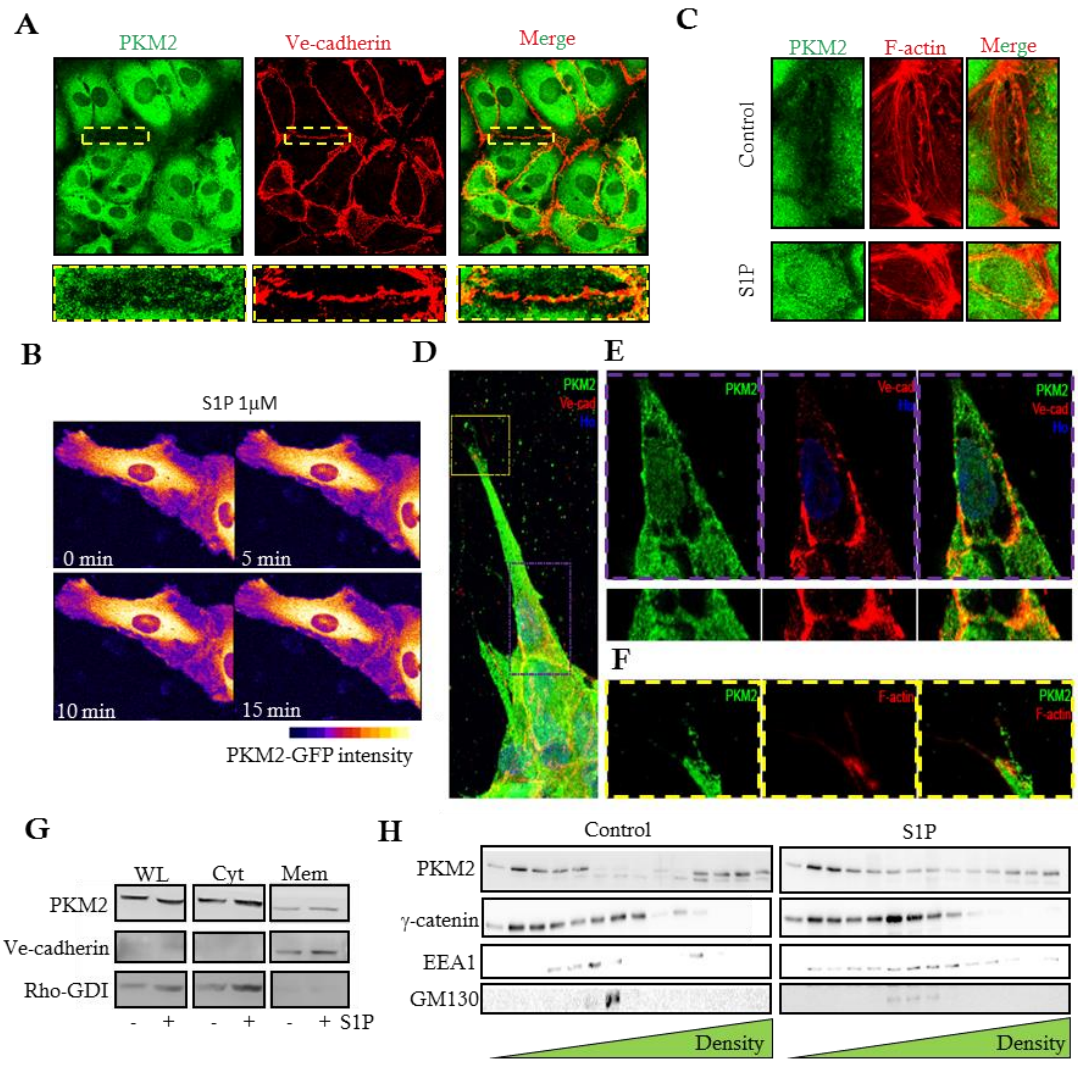

Figure5. PKM2 is located at endothelial cell junctions. A, Representative maximal projections of confocal images of confluent HUVECs interfered for PKM2 or with a control siRNA, stained for Ve-cadherin (red) and PKM2 (green). **B**, PKM2-GFP transfected HUVECs treated with S1P 1μM for 15 min. **C**, Representative maximal projections of confocal images of confluent HUVECs interfered for PKM2 or with a control siRNA, stained for F-actin (red) and PKM2 (green) in basal situation or in S1P-treated cells. **D**, Representative maximal projections of confocal images of sprouts of HUVECs interfered for PKM2 or with a control siRNA, stained for Ve-cadherin (red) and PKM2 (green). **E**, Magnification of D, showing PKM2 and Ve-cadherin colocalization at junctions. **F**, Magnification of D, showing colocalization of PKM2 and F-actin at the filopodia. **G**, Representative western blot of HUVECs subfractionation of cytosol (cyt) and membrane (mem). WL is whole lysate. Expression of PKM2, Ve-cadherin as membrane marker, and Rho-GDI as cytosol marker are shown in HUVECs treated or not with S1P 1μM for 15 min. **H**, Membrane subfractionation in optiprep gradient showing the expression of PKM2, gamma-catenin as plasma membrane marker, EEA1 as endosome marker, and GM130 as Golgi marker in cells treated with S1P or left untreated.

As PKM2 is an enzyme that produces ATP directly, we hypothesize that the observed defects could be produced by a defect in this function at endothelial junctions. First we studied the metabolic state of the interfered cells. The ECAR values that reflect the glycolysis flux were reduced, but not the oxygen consumption, reflecting that the function of the mitochondria remained intact (Figure 6A-C). We analyzed in turn the ATP levels and pyruvate kinase activity in cell fractions obtained by saponin permeabilization, separating cytosol and cytoskeleton-membrane. We tested the different expression of Ve-cadherin and β-actin in those fractions, and found that PKM2 is located at both fractions by Western blot (Figure 6D) and that it is distributed along cytoskeleton after the permeabilization by immunofluorescence (Figure 6E). We discovered that ATP was reduced in the total cell and in both fractions, and the pyruvate kinase activity was decreased in cytosol and in the cytoskeleton-membrane of PKM2 silenced cells, and that the activtity was higher in the cytoskeleton-membrane fraction (Figure 6F-I). This fact could explain that the proliferation was not affected by PKM2, as the lower activity in the cytosol may allow the accumulation of intermediate metabolites of the glycolysis that provide substrates for the proliferation, while in the other locations PKM2 is more active, generating ATP to regulate other processes.

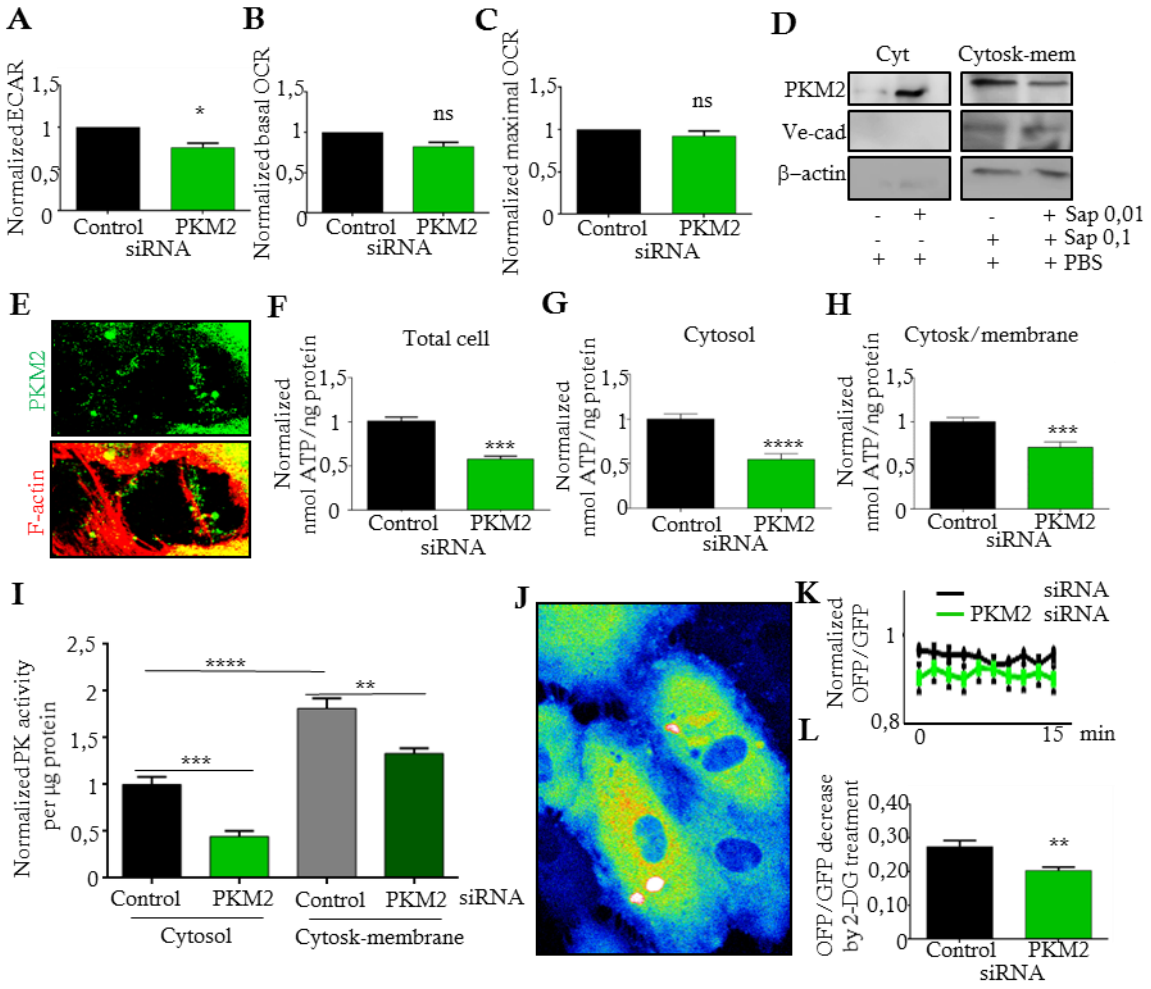

Figure 6. PKM2 regulates ATP local production from glycolysis at endothelial junctions. **A**, Normalized ECAR (extracellular acidification ratio), in PKM2 interfered HUVECs. n=4. **B**, Normalized basal oxygen consumption (OCR) in PKM2-interfered HUVECs. n=4. **C**, Normalized maximal oxygen consumption (OCR) in PKM2-interfered HUVECs. n=4. **D**, Representative western blot of saponin permeabilization in HUVECs. Control situation (-/-) is only PBS. **E**, Representative maximal projections of confocal images of saponin permeabilized HUVECs stained for F-actin (red) and PKM2 (green). **F-H**, Normalized ATP quantification in saponin-permeabilized interfered HUVECs, in total cell (F), cytosol fraction (G) and in cytoskeletal-membrane fraction (H) n=4. **I**, Normalized PK activity per µg of protein quantification in cytosol and cytoskeletal-membrane fractions. n=4. **J**, Representative maximal projections of confocal images of HUVECs expressing Go-aTeam1. **K**, Normalized OFP/GFP fluorescent intensity of Go-aTeam1 in HUVECs interfered for PKM2, along the time. n=4. **L**, OFP/GFP ratio decrease in HUVECs treated with 2mM of 2-Deoxyglucose for 15 min. n=3. ns= no significant; * p<0,05; ** p<0,01; ***p<0,001; **** p<0,0001.

Indeed we also found that the levels of ATP were lower by the observation of a fluorescence construction, GO-aTeam1, which allows the quantification of ATP at subcellular levels (Nakano et al, 2011) (Figure 6J-K). Finally we compared the decrease in the ratio of the GO-aTeam1 by PKM2 interference, with the produced by the inhibition of glycolysis with 2-deoxyglucose (2-DG), a general inhibitor of this metabolic pathway (Chuang et al, 2015). The reduction on the dye ratio produced in PKM2-interfered cells was significantly lower than in control cells, reflecting that this difference were caused by PKM2 and it was similar to the variation obtained in the Figure 6K (Figure 6L).

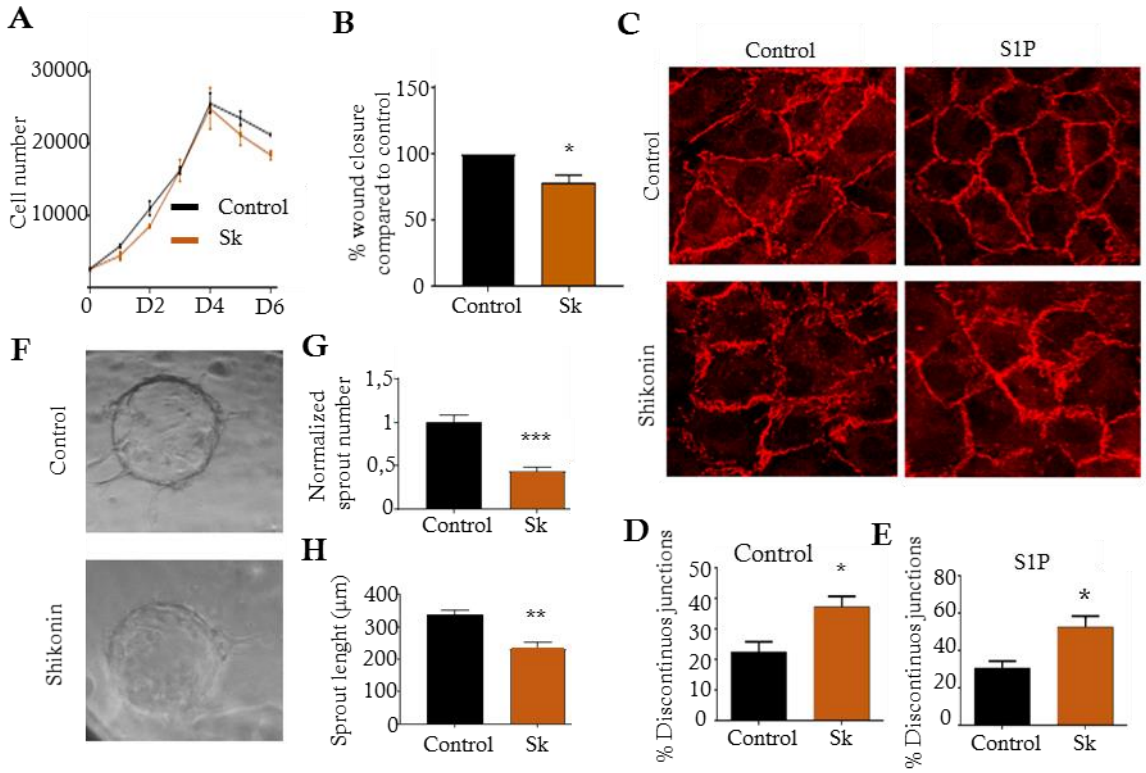

Figure 7. PKM2 inhibition reproduces the effects of PKM2 interference. **A**, HUVEC number along the days in Shikonin (SK) (2µM) treated cells. n=4. **B**, Normalized wound closure in cells treated with SK.n=3. **C**, Representative maximal projections of confocal images of HUVECs stained with Ve-cadherin, treated with SK, and with or without S1P. **D and E**, Quantification of percentage of discontinuous junctions from experiments in C. n=3. **F**, Representative images of brightfield microscopy of spheroids of HUVECs treated with Shikonin. **G**, Normalized sprout number of

spheroid from F. n=3. **H**, Sprout length of spheroids treated with SK. n=3. ns=no significant; * p<0,05; ** p<0,01; ***p<0,001

To test the hypothesis that the reduction of local ATP by the decrease in PKM2 activity is the responsible of the phenotype, we used shikonin, an specific inhibitor of PKM2 isoform (Chen et al, 2011). We found that the migration and the endothelial cell dynamics, but not the proliferation, were affected with the treatment, both in cells in culture and also in the spheroid sprouting assay, so the phenotype observed by the interference approach was reproduced (Figure 7A-H).

PKM2 regulates angiogenesis in vivo

Finally we analyzed the impact of reducing PKM2 in the vascular development in the postnatal mouse retina, by the intravitreal injection of siRNA, which decreased the expression of PKM2 (Figure 8A). We found that the radial vascular growth was reduced, and also the filopodia number in the front (Figures 8B-D). However vascular density was no different (Figure 8E) so we quantified the number of endothelial cells by staining of ERG, a specific nuclear protein of the endothelium, obtaining that the number of positive cells for this marker was the same in the PKM2-silenced retinas (Figure 8F), suggesting that proliferation was no compromised. EC junction pattern was also impaired as the ratio between active and inactive patches of Ve-cadherin was increased in the PKM2 siRNA retinas (Figures 8G-I).

We injected shikonin to test if the inhibition of PKM2 activity could mimic the phenotype of the interference as in the in vitro assays. Thus, radial expansion of retinal vessels was reduced in the treated retinas (Figure 8J) just like filopodia number (Figure 8K). Vascular density and ERG+ cells per area were not different from the DMSO-treated retinas (Figures 8L-M). Finally, EC junction pattern was also compromised (Figures 8N-P).

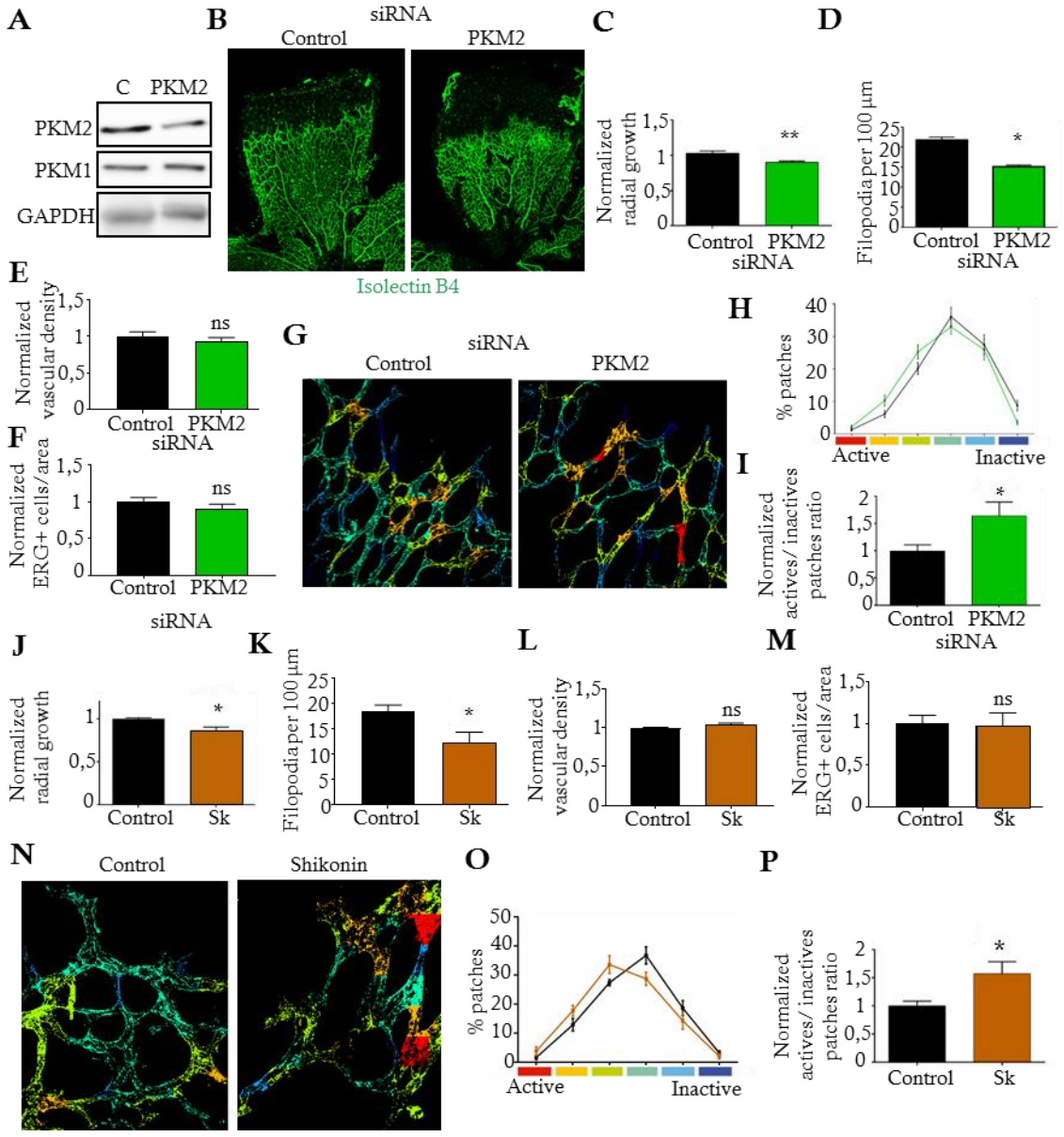

Figure 8. PKM2 activity regulates angiogenesis in vivo. **A**, Representative Western blot of PKM2 interference in retina. **B**, Representative maximal projection of confocal images of retina vessels stained for isolectin B4. **C**, Normalized vessel radial growth quantification in PKM2-interfered retinas. n=8. **D**, Filopodia number per 100 µm of tip cell perimeter in PKM2-interfered retinas; n=4. **E**, Normalized vascular density quantification in PKM2-interfered retinas; n=4. **F**, Normalized ERG+ cells per area in PKM2-interfered retinas; n=4. G, Patching algorithm junction reconstruction of Ve-cadherin staining in PKM2-interfered retinas. n=8. H, Quantification of different types of patches of Ve-cadherin in PKM2-interfered retinas. n=8. **I**, Quantification of active/inactive patches in PKM2-interfered retinas. n=8. **J**, Normalized vessel radial growth quantification in Shikonin (40 µM) treated retinas. n=8. **K**, Filopodia number quantification in Shikonin (40 µM) treated retinas. n=3. **L**, Normalized vascular density in Shikonin (40 µM) treated retinas. n=6. **M**, Normalized ERG+ cells per area in Shikonin (40 µM)-treated retinas. n=6. **N**, Patching algorithm junction reconstruction of Ve-cadherin staining in Shikonin (40 µM) treated retinas. **O**, Quantification of different kind of

patches of Ve-cadherin in Shikonin (40 μM)-treated retinas. n=4. **P**, Quantification of active/inactive patches in Shikonin (40 μM) treated retinas. n=4. ns=not significant; * p<0,05; **p<0,01

In conclusion, we have described the role of PKM2 in angiogenesis, regulating endothelial junctions and cytoskeletal dynamics by local ATP production. Due to the importance of PKM2 in pathologies such as cancer, we provided novel features to take in account to develop new PKM2-based strategies for improvement of treatment for these diseases.

Conclusions

1. The pyruvate kinase isoform that is more expressed in human endothelial cells is PKM2.

2. The endothelial proliferation is not influenced by the expression levels neither by the activity of PKM2.

3. PKM2 regulates the endothelial cells dynamics affecting collective cell migration and the sprouting, “in vitro”.

4. The pyruvate kinase activity is higher in cytoskeletal and membranal subcellular compartments than in cytosol.

5. PKM2 dependent ATP production is also compartmentalized at junctional and cytoskeletal associated regions contributing to the regulation of the functions that occur at that places.

6. The treatment with a specific inhibitor of the M2 pyruvate kinase isoform demonstrates that the activity of PKM2 is necessary for the reorganization of endothelial junctions, migration, and sprouting, “in vitro”.

7. PKM2 regulates the junction dynamics and the cytoskeletal protrusions in endothelial cells affecting “in vivo” vascular development in physiological angiogenesis, with no effects in endothelial proliferation.

Bibliography

Anastasiou, D., G. Poulogiannis, J. M. Asara, M. B. Boxer, J. K. Jiang, M. Shen, G. Bellinger, A. T. Sasaki, J. W. Locasale, D. S. Auld, C. J. Thomas, M. G. Vander Heiden, and L. C. Cantley. 2011. 'Inhibition of pyruvate kinase M2 by reactive oxygen species contributes to cellular antioxidant responses', *Science*, 334: 1278-83.

Bentley, K., C. A. Franco, A. Philippides, R. Blanco, M. Dierkes, V. Gebala, F. Stanchi, M. Jones, I. M. Aspalter, G. Cagna, S. Westrom, L. Claesson-Welsh, D. Vestweber, and H. Gerhardt. 2014. 'The role of differential VE-cadherin dynamics in cell rearrangement during angiogenesis', *Nat Cell Biol*, 16: 309-21.

Boeckel, J. N., A. Derlet, S. F. Glaser, A. Luczak, T. Lucas, A. W. Heumuller, M. Kruger, C. M. Zehendner, D. Kaluza, A. Doddaballapur, K. Ohtani, K. Treguer, and S. Dimmeler. 2016. 'JMJD8 Regulates Angiogenic Sprouting and Cellular Metabolism by Interacting With Pyruvate Kinase M2 in Endothelial Cells', *Arterioscler Thromb Vasc Biol*, 36: 1425-33.

Carmeliet, P., and R. K. Jain. 2011. 'Molecular mechanisms and clinical applications of angiogenesis', *Nature*, 473: 298-307.

Carmeliet, P., M. G. Lampugnani, L. Moons, F. Breviario, V. Compernolle, F. Bono, G. Balconi, R. Spagnuolo, B. Oosthuyse, M. Dewerchin, A. Zanetti, A. Angellilo, V. Mattot, D. Nuyens, E. Lutgens, F. Clotman, M. C. de Ruiter, A. Gittenberger-de Groot, R. Poelmann, F. Lupu, J. M. Herbert, D. Collen, and E. Dejana. 1999. 'Targeted deficiency or cytosolic truncation of the VE-cadherin gene in mice impairs VEGF-mediated endothelial survival and angiogenesis', *Cell*, 98: 147-57.

Chen, J., J. Xie, Z. Jiang, B. Wang, Y. Wang, and X. Hu. 2011. 'Shikonin and its analogs inhibit cancer cell glycolysis by targeting tumor pyruvate kinase-M2', *Oncogene*, 30: 4297-306.

Christofk, H. R., M. G. Vander Heiden, M. H. Harris, A. Ramanathan, R. E. Gerszten, R. Wei, M. D. Fleming, S. L. Schreiber, and L. C. Cantley. 2008. 'The M2 splice isoform of pyruvate kinase is important for cancer metabolism and tumour growth', *Nature*, 452: 230-3.

Chuang, I. C., C. M. Yang, T. Y. Song, N. C. Yang, and M. L. Hu. 2015. 'The anti-angiogenic action of 2-deoxyglucose involves attenuation of VEGFR2 signaling and MMP-2 expression in HUVECs', *Life Sci*, 139: 52-61.

De Bock, K., M. Georgiadou, S. Schoors, A. Kuchnio, B. W. Wong, A. R. Cantelmo, A. Quaegebeur, B. Ghesquiere, S. Cauwenberghs, G. Eelen, L. K. Phng, I. Betz, B. Tembuyser, K. Brepoels, J. Welti, I. Geudens, I. Segura, B. Cruys, F. Bifari, I. Decimo, R. Blanco, S. Wyns, J. Vangindertael, S. Rocha, R. T. Collins, S. Munck, D. Daelemans, H. Imamura, R. Devlieger, M. Rider, P. P. Van Veldhoven, F. Schuit, R. Bartrons, J. Hofkens, P. Fraisl, S. Telang, R. J. Deberardinis, L. Schoonjans, S. Vinckier, J. Chesney, H. Gerhardt, M. Dewerchin, and P. Carmeliet. 2013. 'Role of PFKFB3-driven glycolysis in vessel sprouting', *Cell*, 154: 651-63.

DeBerardinis, R. J., and T. Cheng. 2010. 'Q's next: the diverse functions of glutamine in metabolism, cell biology and cancer', *Oncogene*, 29: 313-24.

Eelen, G., P. de Zeeuw, M. Simons, and P. Carmeliet. 2015. 'Endothelial cell metabolism in normal and diseased vasculature', *Circ Res*, 116: 1231-44.

Fantin, A., A. Lampropoulou, G. Gestri, C. Raimondi, V. Senatore, I. Zachary, and C. Ruhrberg. 2015. 'NRP1 Regulates CDC42 Activation to Promote Filopodia Formation in Endothelial Tip Cells', *Cell Rep*, 11: 1577-90.

Hayer, A., L. Shao, M. Chung, L. M. Joubert, H. W. Yang, F. C. Tsai, A. Bisaria, E. Betzig, and T. Meyer. 2016. 'Engulfed cadherin fingers are polarized junctional structures between collectively migrating endothelial cells', *Nat Cell Biol*, 18: 1311-23.

Hu, H., A. Juvekar, C. A. Lyssiotis, E. C. Lien, J. G. Albeck, D. Oh, G. Varma, Y. P. Hung, S. Ullas, J. Lauring, P. Seth, M. R. Lundquist, D. R. Tolan, A. K. Grant, D. J. Needleman, J. M. Asara, L. C. Cantley, and G. M. Wulf. 2016. 'Phosphoinositide 3-Kinase Regulates Glycolysis through Mobilization of Aldolase from the Actin Cytoskeleton', *Cell*, 164: 433-46.

Israelsen, W. J., T. L. Dayton, S. M. Davidson, B. P. Fiske, A. M. Hosios, G. Bellinger, J. Li, Y. Yu, M. Sasaki, J. W. Horner, L. N. Burga, J. Xie, M. J. Jurczak, R. A. DePinho, C. B. Clish, T. Jacks, R. G. Kibbey, G. M. Wulf, D. Di Vizio, G. B. Mills, L. C. Cantley, and M. G. Vander Heiden. 2013.

'PKM2 isoform-specific deletion reveals a differential requirement for pyruvate kinase in tumor cells', *Cell*, 155: 397-409.

Jones, D. P. 1986. 'Intracellular diffusion gradients of O2 and ATP', *Am J Physiol*, 250: C663-75.

Li, W., J. Liu, K. Jackson, R. Shi, and Y. Zhao. 2014. 'Sensitizing the therapeutic efficacy of taxol with shikonin in human breast cancer cells', *PLoS One*, 9: e94079.

Mazurek, S. 2011. 'Pyruvate kinase type M2: a key regulator of the metabolic budget system in tumor cells', *Int J Biochem Cell Biol*, 43: 969-80.

Menard, L., D. Maughan, and J. Vigoreaux. 2014. 'The structural and functional coordination of glycolytic enzymes in muscle: evidence of a metabolon?', *Biology (Basel)*, 3: 623-44.

Millarte, V., and H. Farhan. 2012. 'The Golgi in cell migration: regulation by signal transduction and its implications for cancer cell metastasis', *ScientificWorldJournal*, 2012: 498278.

Moreno, V., P. Gonzalo, J. Gomez-Escudero, A. Pollan, R. Acin-Perez, M. Breckenridge, M. Yanez-Mo, O. Barreiro, F. Orsenigo, K. Kadomatsu, C. S. Chen, J. A. Enriquez, E. Dejana, F. Sanchez-Madrid, and A. G. Arroyo. 2014. 'An EMMPRIN-gamma-catenin-Nm23 complex drives ATP production and actomyosin contractility at endothelial junctions', *J Cell Sci*, 127: 3768-81.

Nakano, M., H. Imamura, T. Nagai, and H. Noji. 2011. 'Ca(2)(+) regulation of mitochondrial ATP synthesis visualized at the single cell level', *ACS Chem Biol*, 6: 709-15.

Nakatsu, M. N., R. C. Sainson, S. Perez-del-Pulgar, J. N. Aoto, M. Aitkenhead, K. L. Taylor, P. M. Carpenter, and C. C. Hughes. 2003. 'VEGF(121) and VEGF(165) regulate blood vessel diameter through vascular endothelial growth factor receptor 2 in an in vitro angiogenesis model', *Lab Invest*, 83: 1873-85.

Noguchi, T., H. Inoue, and T. Tanaka. 1986. 'The M1- and M2-type isozymes of rat pyruvate kinase are produced from the same gene by alternative RNA splicing', *J Biol Chem*, 261: 13807-12.

Polet, F., and O. Feron. 2013. 'Endothelial cell metabolism and tumour angiogenesis: glucose and glutamine as essential fuels and lactate as the driving force', *J Intern Med*, 273: 156-65.

Serra, H., I. Chivite, A. Angulo-Urarte, A. Soler, J. D. Sutherland, A. Arruabarrena-Aristorena, A. Ragab, R. Lim, M. Malumbres, M. Fruttiger, M. Potente, M. Serrano, A. Fabra, F. Vinals, O. Casanovas, P. P. Pandolfi, A. Bigas, A. Carracedo, H. Gerhardt, and M. Graupera. 2015. 'PTEN mediates Notch-dependent stalk cell arrest in angiogenesis', *Nat Commun*, 6: 7935.

Taniguchi, K., Y. Ito, N. Sugito, M. Kumazaki, H. Shinohara, N. Yamada, Y. Nakagawa, T. Sugiyama, M. Futamura, Y. Otsuki, K. Yoshida, K. Uchiyama, and Y. Akao. 2015. 'Organ-specific PTB1-associated microRNAs determine expression of pyruvate kinase isoforms', *Sci Rep*, 5: 8647.

Tung, J. J., I. W. Tattersall, and J. Kitajewski. 2012. 'Tips, stalks, tubes: notch-mediated cell fate determination and mechanisms of tubulogenesis during angiogenesis', *Cold Spring Harb Perspect Med*, 2: a006601.

Van Daele, P., A. Van Coevorden, P. P. Roger, and J. M. Boeynaems. 1992. 'Effects of adenine nucleotides on the proliferation of aortic endothelial cells', *Circ Res*, 70: 82-90.

Verdegem, D., S. Moens, P. Stapor, and P. Carmeliet. 2014. 'Endothelial cell metabolism: parallels and divergences with cancer cell metabolism', *Cancer Metab*, 2: 19.

Vitorino, P., S. Yeung, A. Crow, J. Bakke, T. Smyczek, K. West, E. McNamara, J. Eastham-Anderson, S. Gould, S. F. Harris, C. Ndubaku, and W. Ye. 2015. 'MAP4K4 regulates integrin-FERM binding to control endothelial cell motility', *Nature*, 519: 425-30.

Xu, M., C. L. Waters, C. Hu, R. B. Wysolmerski, P. A. Vincent, and F. L. Minnear. 2007. 'Sphingosine 1-phosphate rapidly increases endothelial barrier function independently of VE-cadherin but requires cell spreading and Rho kinase', *Am J Physiol Cell Physiol*, 293: C1309-18.

Xu, Q., L. Z. Liu, Y. Yin, J. He, Q. Li, X. Qian, Y. You, Z. Lu, S. C. Peiper, Y. Shu, and B. H. Jiang. 2015. 'Regulatory circuit of PKM2/NF-kappaB/miR-

148a/152-modulated tumor angiogenesis and cancer progression', *Oncogene*, 34: 5482-93.

Yamada, K., T. Noguchi, T. Matsuda, M. Takenaka, P. Monaci, A. Nicosia, and T. Tanaka. 1990. 'Identification and characterization of hepatocyte-specific regulatory regions of the rat pyruvate kinase L gene. The synergistic effect of multiple elements', *J Biol Chem*, 265: 19885-91.

Yu, P., K. Wilhelm, A. Dubrac, J. K. Tung, T. C. Alves, J. S. Fang, Y. Xie, J. Zhu, Z. Chen, F. De Smet, J. Zhang, S. W. Jin, L. Sun, H. Sun, R. G. Kibbey, K. K. Hirschi, N. Hay, P. Carmeliet, T. W. Chittenden, A. Eichmann, M. Potente, and M. Simons. 2017. 'FGF-dependent metabolic control of vascular development', *Nature*, 545: 224-28.

Zala, D., M. V. Hinckelmann, H. Yu, M. M. Lyra da Cunha, G. Liot, F. P. Cordelieres, S. Marco, and F. Saudou. 2013. 'Vesicular glycolysis provides on-board energy for fast axonal transport', *Cell*, 152: 479-91.